Femtosecond polarization shaping of free-electron laser pulses

Giovanni Perosa,[1,2] Jonas Wätzel,[3] David Garzella,[1] Enrico Allaria,[1] Matteo Bonanomi,[4,5] Miltcho Boyanov Danailov,[1] Alexander Brynes,[1] Carlo Callegari,[1] Giovanni De Ninno,[1,6] Alexander Demidovich,[1] Michele Di Fraia,[1,7] Simone Di Mitri,[1,2] Luca Giannessi,[1,8] Michele Manfredda,[1] Luka Novinec,[1] Nitish Pal,[1] Giuseppe Penco,[1] Oksana Plekan,[1] Kevin C. Prince,[1] Alberto Simoncig,[1] Simone Spampinati,[1] Carlo Spezzani,[1] Marco Zangrando,[1,7] Jamal Berakdar,[3] Raimund Feifel,[9] Richard J. Squibb,[9] Ryan Coffee,[10] Erik Hemsing,[10] Eléonore Roussel,[11] Giuseppe Sansone,[12] Brian W. J. McNeil,[13,14,15] and Primož Rebernik Ribič[1,*]

[1] *Elettra-Sincrotrone Trieste, 34149 Basovizza, Trieste, Italy*
[2] *Department of Physics, Università degli Studi di Trieste, 34127 Trieste, Italy*
[3] *Institut für Physik, Martin-Luther-Universität Halle-Wittenberg, 06099 Halle (Saale), Germany*
[4] *Politecnico di Milano, 20133 Milano, Italy*
[5] *Istituto di Fotonica e Nanotecnologie, 20133 Milano, Italy*
[6] *Laboratory of Quantum Optics, University of Nova Gorica, 5001 Nova Gorica, Slovenia*
[7] *Istituto Officina dei Materiali, Consiglio Nazionale delle Ricerche, 34149 Basovizza, Italy*
[8] *ENEA C.R. Frascati, 00044 Frascati (Roma), Italy*
[9] *Department of Physics, University of Gothenburg, 41133 Gothenburg, Sweden*
[10] *SLAC National Accelerator Laboratory, Menlo Park, California 94025, USA*
[11] *Univ. Lille, CNRS, UMR 8523 - PhLAM - Physique des Lasers Atomes et Molécules, F-59000 Lille, France*
[12] *Physikalisches Institut, Albert-Ludwigs-Universität Freiburg, 79085 Freiburg, Germany*
[13] *University of Strathclyde (SUPA), Glasgow G4 0NG, United Kingdom*
[14] *Cockcroft Institute, Warrington, WA4 4AD, United Kingdom*
[15] *ASTeC, STFC Daresbury Laboratory, Warrington, WA4 4AD, United Kingdom*

(Dated: 27th February 2023)

We demonstrate the generation of extreme-ultraviolet (XUV) free-electron laser (FEL) pulses with time-dependent polarization. To achieve polarization modulation on a femtosecond time scale, we combine two delayed counter-rotating circularly polarized pulses from two cross polarized undulators. The polarization profile of the FEL pulses is probed by an infrared laser in above-threshold ionization of helium and the experimental results agree with solutions of the time-dependent Schrödinger equation. We show that the stability limit of the scheme is mainly set by electron beam energy fluctuations, however, at a level that will not compromise experiments in the XUV. Our results demonstrate the potential to improve the resolution and chemical sensitivity of methods based on polarization shaping and may lead to the development of new coherent control schemes for probing and manipulating core electrons in atoms, molecules, and condensed matter.

Generation of laser pulses whose polarization is modulated on a femtosecond time scale is an established technique in the visible spectrum [1, 2]. It has been used in a number of applications, e.g., as an optical centrifuge for rotational acceleration [3] and controlled orientation of molecules [4], to maximize the photoionization yield of diatomic molecules [5, 6], for coherent control of electron wavepackets [7–9] and magnetization [10], for generation of isolated and pairs of attosecond pulses [11, 12], and to improve the sensitivity in multidimensional spectroscopies [13, 14]. The possibility to generate polarization-shaped pulses in the extreme-ultraviolet (XUV) and x-ray spectral regions would improve resolution and chemical sensitivity, and potentially lead to the development of new coherent control methods for probing and manipulating core electrons and associated phenomena.

In the visible, a time-dependent polarization of a laser pulse is accomplished relatively easily using a pulse shaper [15–17]. Due to the lack of efficient optical elements and, in general, due to the difficulties in precisely controlling the propagation of light at short wavelengths, pulse shaping is significantly more complicated in the XUV/x-ray spectral region, especially when it comes to modulating the polarization. Therefore, at such short wavelengths, pulse shapers are practically impossible to fabricate and the only viable options are *in situ* (*i.e.*, during the light generation process itself) techniques. Harmonic conversion of a coherent pulse to shorter wavelengths, and in particular an externally seeded free-electron laser (FEL) such as FERMI [18], where the generated light inherits the properties of the seed (a visible or UV femtosecond laser) [19–21], may provide an answer to the problem of precisely tailoring the spectrotemporal/polarization profile of short and intense XUV/x-ray pulses [22–25].

Experiments demonstrating polarization control of FEL pulses, where the FEL output was circularly or linearly polarized with a purity $> 90\%$, have already been performed at FERMI [26, 27]. However, up to now, the generation of two *delayed* cross polarized pulses (*i.e.*, counter-rotating in the case of circular polarization and perpendicularly polarized in the case of linear polarization), which is one of the simplest ways to achieve a time-

* primoz.rebernik@elettra.eu

This is a peer-reviewed, accepted author manuscript of the following article: Perosa, G., Watzel, J., Garzella, D., Allaria, E., Bonanomi, M., Danailov, M. B., Brynes, A., Callegari, C., De Ninno, G., Demidovich, A., Di Fraia, M., Di Mitri, S., Giannessi, L., Manfredda, M., Novinec, L., Pal, N., Penco, G., Plekan, O., Prince, K. C., ... Ribic, P. R. (2023). Femtosecond polarization shaping of free-electron laser pulses. Physical Review Letters, 131(4), [045001]. https://doi.org/10.1103/PhysRevLett.131.045001

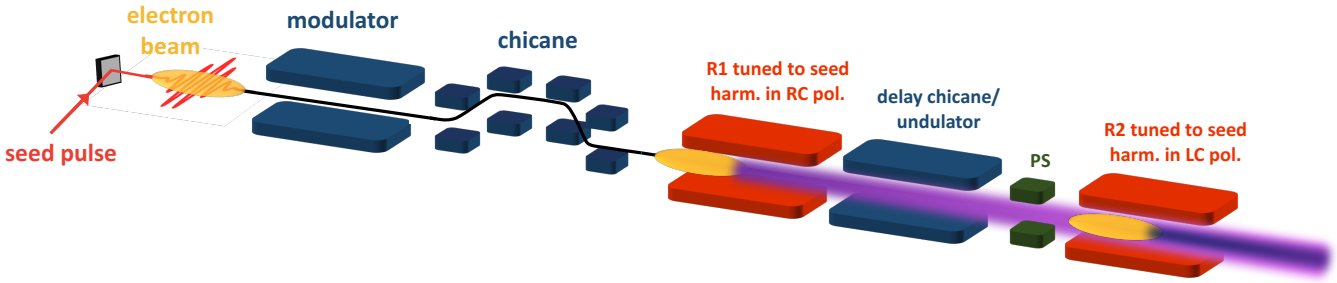

Figure 1: The scheme for generating an XUV FEL pulse with time-dependent polarization. See text for details.

varying polarization, has not yet been demonstrated at an FEL.

Recently, two schemes which are suitable for seeded FELs have been proposed to shape the polarization profile of XUV/x-ray pulses. They are both based on periodically modulating a relativistic electron beam, which is then sent through undulators with alternating polarizations separated by delay chicanes. Such a layout produces two delayed cross polarized pulse trains that coherently add to form an FEL pulse, whose polarization is periodically modulated on a femtosecond or even attosecond time scale [28–30]. Here, we propose and experimentally demonstrate a simplified method, where instead of pulse trains we use single FEL pulses.

The layout for generating FEL pulses with time-dependent polarization is sketched in Fig. 1. After interacting with the seed laser in the modulator and traversing a magnetic chicane just as in a standard high-gain harmonic generation (HGHG) FEL [31], the microbunched portion of the electron beam emits a right-circularly (RC) polarized FEL pulse at an integer harmonic of the seed frequency in the downstream radiator R1. The electron beam is then delayed with respect to this FEL pulse using a highly dispersive element (delay chicane or undulator tuned to a non-integer harmonic of the seed). It then traverses R2, generating a left-circularly (LC) polarized FEL pulse, *i.e.*, counter-rotating with respect to the first one. A phase shifter PS (a small chicane) located just before R2 is used to fine tune the relative phase between the two cross polarized FEL sub-pulses. Having variable-polarization radiators [26], the same setup also allows generating two linearly polarized sub-pulses with orthogonal polarizations.

The calculated properties of the output pulse (assuming two identical, cross polarized Gaussian pulses separated in time) are shown in Fig. 2 for a delay between the sub-pulse envelopes of one full width half maximum (FWHM = 60 fs) of the sub-pulse duration and a relative phase of $\pi/4$. The left panel shows the on-axis x and y components of the total electric field E_x, E_y and the total intensity I. Unlike pulses with time-independent polarization (e.g., pure circular), the resulting pulses have time-dependent Stokes parameters, which are in general all different from zero - see right panel in Fig. 2 (the Stokes parameters were normalized with respect to $S_0 = I$). For the parameters used in Fig. 2, the polarization evolves from RC in the pulse head ($t < -50$ fs), to linear in the pulse center ($t = 0$), and to LC in the pulse tail ($t > 50$ fs).

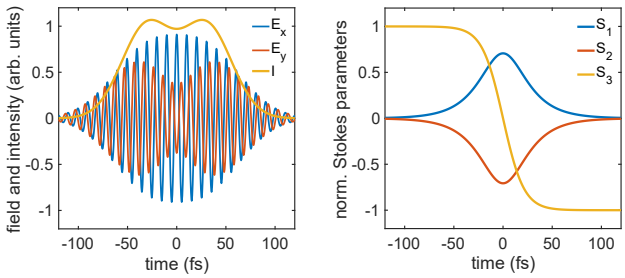

Figure 2: Schematic output of the setup shown in Fig. 1 for a separation between the sub-pulse envelopes equal to their FWHM durations (60 fs) and a relative phase of $\pi/4$. Left: components of the total electric field and total intensity. The FEL wavelength is exaggerated to visualize oscillations of the fields. Right: temporal profiles of the normalized Stokes parameters.

Varying the relative phase between the sub-pulses is a convenient way to control the Stokes parameters of the composite pulse, in particular the direction of the (purely linear) polarization at $t = 0$. When this phase is modified, the electric field rotates in the polarization plane. However, this also means that any unwanted phase fluctuations between the two sub-pulses will lead to a fluctuating output polarization. In an FEL, such fluctuations are a consequence of electron beam energy fluctuations (due to fluctuating radio frequency fields used to accelerate the beam), which are converted into trajectory fluctuations when the electrons propagate through magnetic fields in dispersive regions of the FEL line. Because the amount of dispersion that is used to delay the sub-pulses depends on the electron beam energy, shot-to-shot energy fluctuations will result in shot-to-shot phase fluctuations between the two sub-pulses that might prevent the realization of the scheme. Even if the dispersion is set to zero, we expect residual phase fluctuations between the sub-pulses due to electron-beam trajectory jitter along the FEL line.

To characterize the phase fluctuations, we first operated FERMI [18] at the sixth harmonic of a 250 nm seed ($\lambda_{FEL} \approx 42$ nm) in a co-rotating configuration with R1 (two radiator modules) and R2 (one module) both tuned to RC polarization and measured the output intensity as a function of the relative phase between the sub-pulses. The sub-pulse duration estimated from the seed duration (120 fs) was 60 fs [22, 32]. The measurement was performed with balanced peak electric fields of the sub-pulses and sampling the FEL beam through a 2.5 mm × 2.5 mm aperture located ∼ 50 m downstream of R2 to limit off-axis effects due to different wavefront curvatures of radiation emitted in R1 and R2. Fig. 3, top shows the normalized intensity $2I/(I_{min} + I_{max})$ as a function of the additional phase generated by PS for zero (left) and 30 fs (right) delay between the sub-pulse envelopes. For zero delay, we observe a maximum (minimum) at $\sim 0.2\lambda$ ($\sim 0.7\lambda$), corresponding to constructive (destructive) interference between the sub-pulses [33]. From a simple model using two Gaussian pulses whose sources are separated in space (10 m separation, 100 μm source sizes) and time, the expected contrast is higher (red curve). However, including a typical electron beam trajectory jitter along the FEL line [34], the experiment agrees well with the model (yellow curve). Delaying the pulses by 0.5×FWHM of the sub-pulse duration, the experimental contrast is further reduced, partly because interference now occurs only in the overlap region, but mostly due to additional phase fluctuations introduced by the undulator that delays the sub-pulses (note the larger error bars). In this case, the theoretical prediction matches the measurements after including relative electron beam energy fluctuations on the order of 4×10^{-4}, corresponding well to the measured values at FERMI.

The root-mean-square phase fluctuations in Fig. 3 correspond to $\approx 0.06\lambda$ and $\approx 0.17\lambda$, for zero and 30 fs delay, respectively and are not expected to compromise the proposed scheme. This is further demonstrated for counter-rotating fields (producing the output in Fig. 2) by tuning R2 to LC polarization. In this case, the FEL intensity does not depend on the relative phase. We therefore evaluated the fluctuations by measuring photoelectron distributions from He atoms excited by such FEL pulses using a velocity map imaging (VMI) detector that is sensitive to the polarization of light [35, 36]. We first acquired VMI images for pure linear horizontal and vertical polarizations L_H and L_V and assumed that for an arbitrary polarized FEL pulse (also the one in Fig. 2), the VMI image IM can be decomposed as their weighted sum $IM = a_H L_H + a_V L_V$, where $a_H, a_V \geq 0$ [37]. We then evaluated the difference-sum ratio $DSR = (a_H - a_V)/(a_H + a_V)$ as a function of the relative phase between the sub-pulses (Supplemental Material). The comparison between the experimental DSR and the one obtained by solving the time-dependent Schrödinger equation (TDSE) and projecting the photoelectron distributions onto the horizontal and vertical components (Supplemental Material) is shown in Fig. 3, bottom. For zero delay (left), the

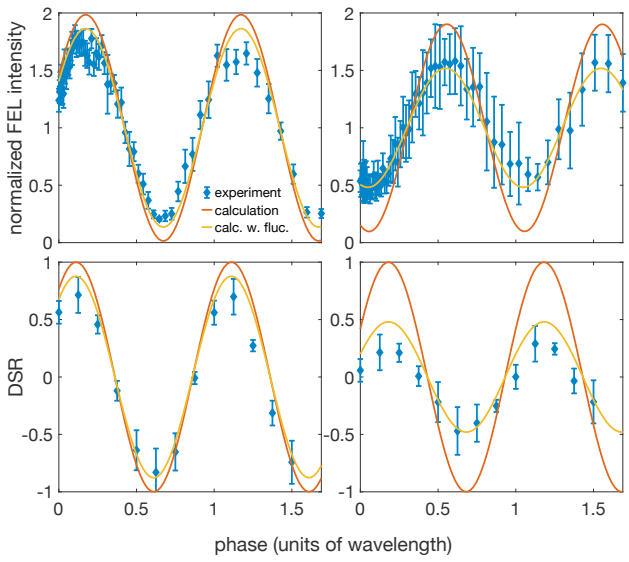

Figure 3: FEL intensity for co-rotating sub-pulses (top) and DSR obtained from decomposition of VMI images for counter-rotating sub-pulses (bottom) as a function of additional phase (generated by PS before R2 in Fig. 1) for zero (left) and 30 fs (right) delay between the sub-pulse envelopes. Error bars indicate ± one standard deviation and are calculated from 50 measurements (top) and confidence intervals obtained during image decomposition (bottom).

experimental DSR is less than the theoretical one (red curve), however, after including phase fluctuations at the same level ($\approx 0.06\lambda$) as for the co-rotating case, the theory (yellow curve) matches well with the experiment. For this cross polarized configuration at zero delay, the maximum (minimum) signal at $\sim 0.1\lambda$ ($\sim 0.6\lambda$) corresponds to horizontal (vertical) polarization. As expected, the DSR is reduced for a 30 fs delay between the sub-pulses (right panel) due to additional fluctuations introduced by the delay undulator. Also here, after including the phase fluctuations at a level of $\approx 0.17\lambda$ (the same as for the co-rotating case), the theory agrees relatively well with the experiment, demonstrating that the main factor that decreases the DSR are electron beam energy fluctuations. For the 30 fs delay, the maximum (minimum) signal corresponds to horizontal (vertical) polarization in the overlap region ($t \sim 0$ fs).

The above results demonstrate the practical relevance of electron beam energy/trajectory fluctuations, but also that they are at a level that will not compromise potential experiments, as shown by the non-vanishing DSR in the bottom right panel of Fig. 3. The phase stability can be further increased by decreasing the FEL pulse duration (using a shorter seed), allowing to reduce the sub-pulse delay or by implementing the scheme at an FEL driven by a superconducting linear accelerator with lower shot-to-shot electron beam energy fluctuations [38]. In addition,

by monitoring the beam position in dispersive regions of the FEL line during the experiment, the data can be sorted with respect to the electron beam energy in post-processing.

Because the phase fluctuations increase with the sub-pulse delay, the results in Fig. 3 are (indirect) evidence that we are indeed producing two delayed FEL pulses that will generate the FEL output shown in Fig. 2 in the counter-rotating configuration. For a more direct demonstration of the pulse structure in Fig. 2, we resorted to above-threshold ionization (ATI) in the presence of an optical dressing field. For this purpose, we spatially and temporally overlapped the FEL pulse with a short ($\sim$ 15 fs FWHM) and intense ($\sim 10^{13}$ W/cm^2) linearly polarized infrared (IR) laser ($\lambda \approx 800$ nm). The IR field gives rise to sidebands in the photoelectron spectra (separated by the IR photon energy), which correspond to additional absorption or stimulated emission of optical photons by the XUV-generated photoelectrons [39]. We acquired electrons from photoionization of He atoms as a function of the delay between the FEL and IR pulses using a magnetic bottle spectrometer (no angular resolution required this time) [40]. In such a cross-correlation experiment [39, 41], the IR probe pulse duration determines the length of the pulse structures that can still be resolved. For this set of experiments, the FEL sub-pulse duration estimated from the 70 fs seed duration [22, 32] and confirmed by cross-correlation measurements was 40 fs. Because our IR pulse was only $\sim 3\times$ shorter than the FEL sub-pulse, we analyzed the third sideband to reduce the effective probe pulse duration [32, 41] and increase the temporal resolution.

The cross-correlation measurements (see Supplemental Material on how the data was processed) for a delay between the FEL sub-pulse envelopes of 25 and 41 fs as a function of the relative phase between the sub-pulses are shown in the top and bottom left panels of Fig. 4, respectively. For the 25 fs delay, the photoelectron signal varies by changing the relative phase. In the center of the FEL pulse, the polarization is linear (see Fig. 2) and its direction rotates as a function of the phase, *i.e.*, it varies from being parallel to the IR polarization, where we observe the maximum photoionization (PE) yield, to being perpendicular to the IR polarization, where the minimum PE yield is observed. Such a variation of the photoelectron signal vs. the relative angle between the XUV and IR polarization vectors is expected based on angular momentum conservation rules [39].

Looking at the cross-correlation signal in the top left panel of Fig. 4, we see (Supplemental Material) that its shape can be described by two Gaussians separated by around 30 fs, which is close to the sub-pulse delay. For the 41 fs separation (bottom left panel), the variation of the PE yield vs. relative phase is observed again and is more restricted to the central part of the cross-correlation signal, where the pulse is linearly polarized. In this case, two peaks can be clearly resolved due to the increased separation (around 40 fs), which corresponds well to the sub-pulse delay.

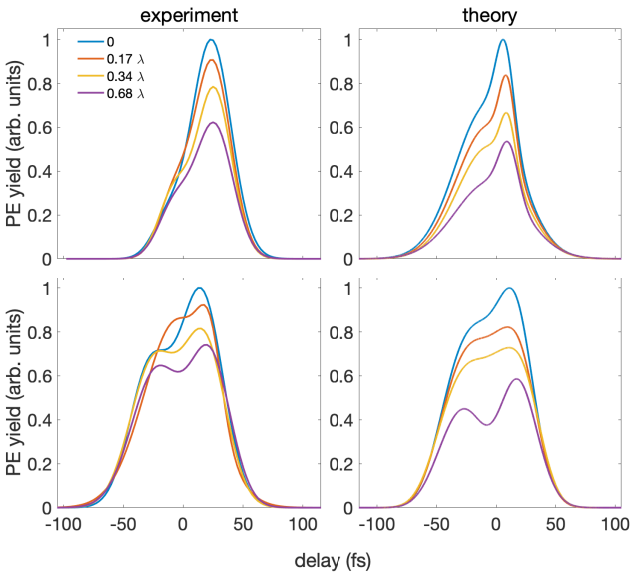

Figure 4: Experimental (left) and theoretical (right) total PE yields corresponding to the third sideband as a function of the delay between the FEL and IR pulses for different values of the relative phase between the FEL sub-pulses. The delay between the sub-pulse envelopes was 25 fs (top) and 41 fs (bottom).

The experimental PE yields agree well with the results of TDSE calculations (Supplemental Material) shown in the right panels of Fig. 4. The asymmetric shapes observed both in experiment and theory are due to the fact that the second sub-pulse is longer ($\sim$ 55 fs compared to 40 fs for the first sub-pulse), because the electron beam travels through the delay chicane [22, 32] - different sub-pulse durations have a negligible effect on the results in Fig. 3. A weaker variation of the PE yield vs. phase in the calculations compared to the experiment (especially for a 41 fs delay) is attributed to additional phase fluctuations introduced by the power supply of the magnetic chicane, which could not be measured on a shot-to-shot basis and were not included in the simulations (in Fig. 3, the delay was introduced using an undulator with permanent magnets).

Fig. 4 provides additional evidence that the two FEL sub-pulses are phase-locked, otherwise no variation of the PE yield vs. phase would be observed in the ATI experiments. Therefore, the fact that we have generated a linearly polarized pulse region, whose polarization direction depends on the phase shift between the FEL sub-pulses and whose extent (compared to the total FEL pulse duration) depends on the sub-pulse separation, together with the fact that we observe two peaks in the cross-correlation traces, can only mean that we have indeed generated two counter-rotating phase-locked sub-pulses that coherently add to form an FEL pulse with time-dependent polarization, such as the one shown in Fig. 2.

Our scheme can be relatively easily implemented at existing seeded FEL facilities. It will allow extending methods based on polarization shaping into the XUV regime. These include, among others, the production of electron vortices using single photon photoionization [42], coherent control of electron wave packets [43], and observing photoelectron circular dichroism within a single measurement [44].

ACKNOWLEDGMENTS

This work was in part supported by the DFG (project no. 429194455). R.F. acknowledges financial support from the Swedish Research Council and the Knut and Alice Wallenberg Foundation, Sweden. The work of E.H. was supported by U.S. Department of Energy Award no. 2021-SLAC-100732. G.S. acknowledges financial support from the Deutsche Forschungsgemeinschaft Research Training Group DynCAM (RTG 2717) and grant 429805582 (project SA 3470/4-1).

[1] K. Misawa, Applications of polarization-shaped femtosecond laser pulses, Adv. in Phys. **1**, 544 (2016).
[2] H. Qi, Z. Lian, D. Fei, Z. Chen, and Z. Hu, Manipulation of matter with shaped-pulse light field and its applications, Adv.in Phys. **6**, 1949390 (2021).
[3] D. M. Villeneuve *et al.*, Forced molecular rotation in an optical centrifuge, Phys. Rev. Lett. **85**, 542 (2000).
[4] A. A. Milner *et al.*, Controlled enantioselective orientation of chiral molecules with an optical centrifuge, Phys. Rev. Lett. **122**, 223201 (2019).
[5] T. Brixner *et al.*, Quantum control by ultrafast polarization shaping, Phys. Rev. Lett. **92**, 208301 (2004).
[6] T. Suzuki, S. Minemoto, T. Kanai, and H. Sakai, Optimal control of multiphoton ionization processes in aligned $\mathbf{I_2}$ molecules with time-dependent polarization pulses, Phys. Rev. Lett. **92**, 133005 (2004).
[7] D. Pengel *et al.*, Electron vortices in femtosecond multiphoton ionization, Phys. Rev. Lett. **118**, 053003 (2017).
[8] K. Eickhoff *et al.*, Multichromatic polarization-controlled pulse sequences for coherent control of multiphoton ionization, Front. Phys. **9**, 675258 (2021).
[9] N. Dudovich *et al.*, Quantum control of the angular momentum distribution in multiphoton absorption processes, Phys. Rev. Lett. **92**, 103003 (2004).
[10] N. Kanda *et al.*, The vectorial control of magnetization by light, Nat. Comm. **2**, 362 (2011).
[11] G. Sansone *et al.*, Isolated single-cycle attosecond pulses, Science **314**, 443 (2006).
[12] G. Sansone *et al.*, Shaping of attosecond pulses by phase-stabilized polarization gating, Phys. Rev. A **80**, 063837 (2009).
[13] J. A. Myers, K. L. M. Lewis, P. F. Tekavec, and J. P. Ogilvie, Two-color two-dimensional fourier transform electronic spectroscopy with a pulse-shaper, Opt. Express **16**, 17420 (2008).
[14] S.-H. Shim and M. T. Zanni, How to turn your pump–probe instrument into a multidimensional spectrometer: 2d IR and Vis spectroscopies via pulse shaping, Phys. Chem. Chem. Phys. **11**, 737 (2009).
[15] T. Brixner and G. Gerber, Femtosecond polarization pulse shaping, Opt. Lett. **26**, 557 (2001).
[16] P. S. O. Masihzadeh and R. Bartels, Complete polarization state control of ultrafast laser pulses with a single linear spatial light modulator, Opt. Express **15**, 18025 (2007).
[17] T. S. M. Sato and K. Misawa, Interferometric polarization pulse shaper stabilized by an external laser diode for arbitrary vector field shaping, Rev. Sci. Instrum. **80**, 123107 (2009).
[18] E. Allaria *et al.*, Highly coherent and stable pulses from the FERMI seeded free-electron laser in the extreme ultraviolet, Nat. Photonics **6**, 699 (2012).
[19] O. Y. Gorobtsov *et al.*, Seeded x-ray free-electron laser generating radiation with laser statistical properties, Nat. Commun **9**, 4498 (2018).
[20] P. R. Ribič *et al.*, Coherent soft x-ray pulses from an echo-enabled harmonic generation free-electron laser, Nat. Photonics **13**, 555 (2019).
[21] G. Penco *et al.*, Nonlinear harmonics of a seeded free-electron laser as a coherent and ultrafast probe to investigate matter at the water window and beyond, Phys. Rev. A **105**, 053524 (2022).
[22] D. Gauthier *et al.*, Spectrotemporal shaping of seeded free-electron laser pulses, Phys. Rev. Lett. **115**, 114801 (2015).
[23] D. Gauthier *et al.*, Generation of phase-locked pulses from a seeded free-electron laser, Phys. Rev. Lett. **116**, 024801 (2016).
[24] N. S. Mirian *et al.*, Spectrotemporal control of soft x-ray laser pulses, Phys. Rev. Accel. Beams **23**, 060701 (2020).
[25] P. K. Maroju *et al.*, Attosecond pulse shaping using a seeded free-electron laser, Nature **578**, 386 (2020).
[26] E. Allaria *et al.*, Control of the polarization of a vacuum-ultraviolet, high-gain, free-electron laser, Phys. Rev. X **4**, 041040 (2014).
[27] E. Ferrari *et al.*, Free electron laser polarization control with interfering crossed polarized fields, Phys. Rev. Accel. Beams **22**, 080701 (2019).
[28] N. Sudar, R. Coffee, and E. Hemsing, Coherent x rays with tunable time-dependent polarization, Phys. Rev. Accel. Beams **23**, 120701 (2020).
[29] J. Morgan and B. W. J. McNeil, Attosecond polarization modulation of x-ray radiation in a free-electron laser, Phys. Rev. Accel. Beams **24**, 010701 (2021).
[30] J. Morgan and B. W. J. McNeil, X-ray pulse generation with ultra-fast flipping of its orbital angular momentum, Opt. Express **30**, 31171 (2022).
[31] L. H. Yu, Generation of intense uv radiation by subharmonically seeded single-pass free-electron lasers, Phys. Rev. A **44**, 5178 (1991).
[32] P. Finetti *et al.*, Pulse duration of seeded free-electron lasers, Phys. Rev. X **7**, 021043 (2017).
[33] Note that the zero phase of PS is not calibrated and is different for all the plots, because the FEL required a

reoptimization of operating parameters for each of the configurations.
[34] 50 μm root mean square in both directions in the plane perpendicular to the beam propagation at each position monitor placed between the undulator sections.
[35] P. O'Keeffe *et al.*, A photoelectron velocity map imaging spectrometer for experiments combining synchrotron and laser radiations, Rev. Sci. Instrum. **82**, 033109 (2011).
[36] P. O'Keeffe *et al.*, A velocity map imaging apparatus for gas phase studies at FERMI@Elettra, Nucl. Instrum. Methods Phys. Res. B **284**, 69 (2012).
[37] S. T. Manson and A. F. Starace, Photoelectron angular distributions: energy dependence for *s* subshells, Rev. Mod. Phys. **54**, 389 (1982).
[38] W. Decking *et al.*, A MHz-repetition-rate hard x-ray free-electron laser driven by a superconducting linear accelerator, Nat. Photonics **14**, 391 (2020).
[39] M. Meyer *et al.*, Two-colour experiments in the gas phase, J. Phys. B: At. Mol. Opt. Phys. **43**, 194006 (2010).
[40] P. Kruit and F. H. Read, Magnetic field paralleliser for 2π electron-spectrometer and electron-image magnifier, J. Phys. E: Sci. Instrum. **16**, 313 (1983).
[41] A. Bouhal *et al.*, Cross-correlation measurement of femtosecond noncollinear high-order harmonics, J. Opt. Soc. Am. B **14**, 950 (1997).
[42] J. M. N. Djiokap *et al.*, Electron vortices in photoionization by circularly polarized attosecond pulses, Phys. Rev. Lett. **115**, 113004 (2015).
[43] M. Wollenhaupt *et al.*, Interferences of ultrashort free electronwave packets, Phys. Rev. Lett. **89**, 173001 (2002).
[44] P. V. Demekhin *et al.*, Photoelectron circular dichroism with two overlapping laser pulses of carrier frequencies ω and 2ω linearly polarized in two mutually orthogonal directions, Phys. Rev. Lett. **121**, 253201 (2018).